Journal of Applied Physics

Modeling energy exchange and heating within nanorod arrays due to near-field radiative coupling

Cite as: J. Appl. Phys. **127**, 234302 (2020); https://doi.org/10.1063/5.0005421
Submitted: 21 February 2020 . Accepted: 28 May 2020 . Published Online: 16 June 2020

Kevin J. Voon, Mike Chang, George A. Sawatzky, and Alireza Nojeh

Journal of Applied Physics ARTICLE scitation.org/journal/jap

Modeling energy exchange and heating within nanorod arrays due to near-field radiative coupling

Cite as: J. Appl. Phys. **127**, 234302 (2020); doi: 10.1063/5.0005421
Submitted: 21 February 2020 · Accepted: 28 May 2020 ·
Published Online: 16 June 2020

Kevin J. Voon,[1,2,a)] Mike Chang,[1,2] George A. Sawatzky,[2,3,4] and Alireza Nojeh[1,2]

AFFILIATIONS

[1]Department of Electrical and Computer Engineering, University of British Columbia, Vancouver, BC V6T 1Z4, Canada
[2]Quantum Matter Institute, University of British Columbia, Vancouver, BC V6T 1Z4, Canada
[3]Department of Physics and Astronomy, University of British Columbia, Vancouver, BC V6T 1Z1, Canada
[4]Department of Chemistry, University of British Columbia, Vancouver, BC V6T 1Z1, Canada

[a)]**Author to whom correspondence should be addressed:** kvoon@ece.ubc.ca

ABSTRACT

We present a heat transfer model to obtain the temperature distribution within aligned nanorod arrays. The model includes thermal conduction along each nanorod in addition to a phenomenological treatment of near-field radiative energy exchange among the nanorods and allows us to investigate the interplay between these effects. The contribution of the near-field radiative energy exchange to overall heating is found to increase significantly with a decrease in inter-nanorod spacing and an increase in array size; the effect is also more prominent for nanorods with lower thermal conductivity and higher emissivity.

INTRODUCTION

Understanding energy exchange among nanostructures is important for various electronic and thermal applications using nanomaterials, such as energy conversion and thermal management.[1–4] Radiative energy exchange is particularly prominent at sub-wavelength distances between transmitting surfaces (less than ~10 μm apart for infrared radiation).[5] Within those distances, near-field coupling of surface plasmon polaritons or phonon polaritons due to evanescent waves (also referred to as photon tunneling) leads to a nonlinear increase in energy exchange with decreasing inter-surface distances.[5–7] Experimental works have reported enhancement factors of two orders of magnitude for distances of around 100 nm as compared to the equivalent energy exchange when only considering far-field radiation.[8,9] For distances of around 10 nm, theoretical studies based on fluctuational electrodynamics have predicted above three orders of magnitude enhancement in radiative transfer.[5,10,11]

Heating of individual nanotubes has been modeled in the past.[12] Because of strong interactions, radiative energy exchange is a critical consideration in analyzing heat flow within collections of nanotubes and nanowires, whether in small bundles or in macroscopic assemblies. For example, an intriguing phenomenon in this context is the strong heat localization (the Heat Trap effect) in arrays of aligned carbon nanotubes (CNT forests), which has promising applications in thermionic and thermoelectric energy conversion and vacuum nanoelectronics.[13–15]

In this work, we study the effect of near-field radiative coupling on temperature distribution within arrays of nanorods. We present a phenomenological model for near-field radiative coupling among the nanorods based on results on two-body interactions available in the literature.[11] Given the wide range of values of thermal conductivity and optical properties of various nanowires and nanotubes,[1,2,5,16] we also investigate how these properties affect heat transport within the array.

MODEL AND RESULTS

One nanorod

Each nanorod was modeled as a solid cylindrical thermal conductor (Fig. 1), with heat transport governed by the one-dimensional time-independent heat equation,

$$\frac{d}{dz}\left(k(n)\frac{dT(n)}{dz}\right) + Q_{\text{in}}(n) - Q_{\text{rad}}(n) = 0, \tag{1}$$

where k is the thermal conductivity, and Q_{in} and Q_{rad} are the volumetric power densities delivered to and leaving element n with length dz, respectively. Q_{in} could be due to optical heating or

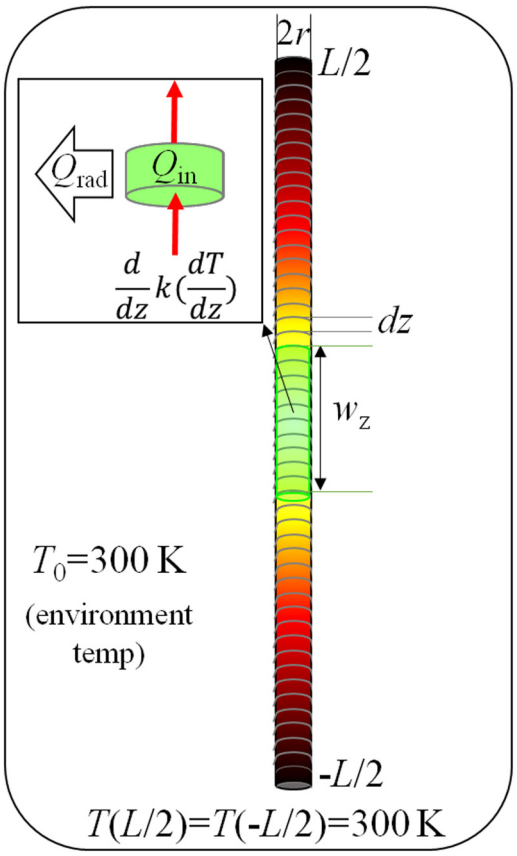

FIG. 1. Schematic showing finite difference discretization for one nanorod in vacuum. The inset shows the heat flow components acting on a single element with length *dz*, as depicted in Eq. (1). Here, w_z is the width of the Q_{in} profile.

resistive heating, while Q_{rad} is a purely radiative term. We do not include convection in the model as the material is assumed to be in vacuum. The equation was solved using the finite difference method, with the nanorod discretized into equally spaced elements along its length *L*. This approach is similar to that described in Ref. 38 and Ref. 12. Dirichlet boundary conditions of $T(-L/2) = T(L/2) = 300$ K were applied, implying contact with room-temperature thermal baths (such as highly thermally conductive substrates held at room temperature) on both ends. A wide range of thermal conductivity models, including constant values in the range of $k = 1 - 5000$ W/m K as well as a temperature-dependent one,[17] were used to investigate how *k* affects temperature distribution. This is because thermal conductivity of nanostructures can vary significantly due to factors such as defects or phonon quenching in bundles.[5,18–21] For example, CNT thermal conductivity values of 0.1 W/m K to 3 500 W/m K have been reported from experimental measurements, with even higher values predicted from modeling.[1,2,17,19,21,22]

The treatment of Q_{rad} reflects a given nanorod's interactions with other nanorods and the outer environment. For a single nanorod suspended in vacuum, we assume Q_{rad} to be given by the Stefan–Boltzmann equation

$$Q_{rad}(n) = \sigma\varepsilon(l/A)\left[T(n)^4 - T_0^4\right], \tag{2}$$

where σ is the Stefan–Boltzmann constant, ε is the emissivity of the nanorod (which is equal to its absorptivity in thermal equilibrium), *l* and *A* are the cross-sectional circumference and area of the nanorod, respectively, and the environment temperature T_0 is 300 K.

We recognize that, since the nanorod radius is significantly smaller than the thermal wavelength, the actual radiated power may deviate significantly from the value estimated using the Stefan–Boltzmann formula. For example, it has been predicted that thermal emission may be up to two orders of magnitude weaker or stronger than the Stefan–Boltzmann value for nanoscale dielectric and metallic cylinders, respectively, with the effect strongly dependent on radius.[23] These deviations may be accounted for by having ε also serve as an approximate correction factor.[24] We thus carried out simulations with a wide range of ε values in order to capture the possible variances in temperature and radiative energy exchange due to this effect.

As a first step, in order to establish insight into the levels of power and temperature involved in experiments, a single nanorod was simulated under the conditions described in the experiments of Liu *et al.* on individual CNTs.[25] For a 10-μm-long CNT, in Ref. 25, the Q_{in} profile was due to a Gaussian laser beam with a $1/e^2$ beam diameter of 0.98 μm delivering a total power of 93.2 nW to the CNT and resulting in a peak temperature of 353 K. Using the same Q_{in} profile, we obtained a simulated temperature of 351 K, in close agreement with the above measured value of Ref. 25

We now turn to a systematic study of the effect of thermal conductivity. The emissivity value was set to $\varepsilon = 0.09$, inspired by the assumed emissivity of a double-walled CNT (equivalent to four graphene sheets, each with $\varepsilon \sim 2.3\%$[26]). The radius was set to $r = 5$ nm, the length to $L = 1$ mm, and Q_{in} was uniformly distributed over the central 200 μm portion of the nanorod.

Figure 2(a) shows the peak temperature as a function of total heating power for various constant thermal conductivity values in the range of $k = 1 - 5000$ W/m K. As shown in the graph, below 100 W/m K, the temperature is not sensitive to thermal conductivity, indicating that thermal radiation becomes the dominant energy loss mechanism. This was also observed for a particular temperature-dependent thermal conductivity model reported for CNTs [see Fig. 2(a) for details],[17] for which the relation of peak temperature with total power bridged the high-*k* and low-*k* limits. Above a thermal conductivity of 500 W/m K, the temperature profile [Fig. 2(b)] was pyramid-shaped due to thermal conduction being the primary means of heat dissipation. With lower thermal conductivity, the reduced heat dissipation led to the temperature profile closely resembling the Q_{in} profile in shape, with a virtually uniform temperature along the middle 200 μm section receiving energy from Q_{in} that would rapidly transition to room temperature outside that region, where Q_{in} was 0. Similar trends were observed for much lower and higher emissivity values, only with higher and

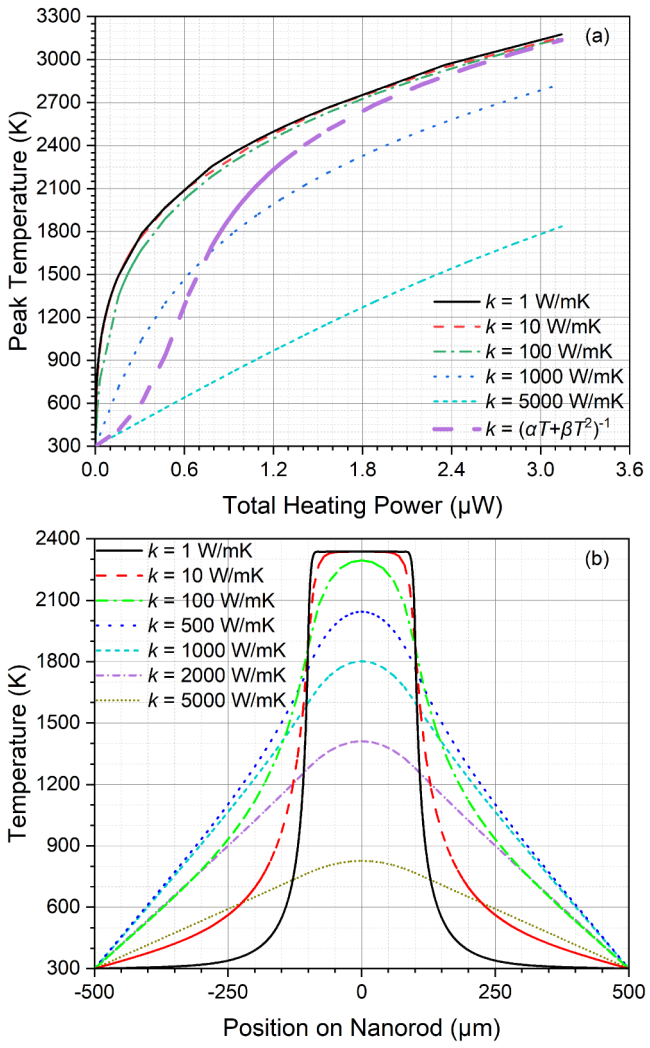

FIG. 2. (a) Peak nanorod temperature as a function of total heating power for various thermal conductivity values, including a nonlinear k model of $k = (\alpha T + \beta T^2)^{-1}$ where $\alpha = 3.7 \times 10^{-7}$ m/W and $\beta = 9.7 \times 10^{-10}$ m/W K as reported in Ref. 17. (b) Temperature distribution along the nanorod for a total absorbed heating power of 0.94 μW and various thermal conductivity values.

lower temperatures, respectively, for the same Q_{in} (see Figs. S1 and S2 in the supplementary material).

Two nanorods

In the case of two nanorods, we modeled Q_{rad} as

$$Q_{rad}(n) = F_{NF}\sigma\varepsilon(l/A)\left[T_1(n)^4 - T_2(n)^4 F_V - T_0^4(1 - F_V)\right], \quad (3)$$

where F_V is the view factor, or the percentage of radiation transferred between nanorods, with the portion of radiation not absorbed by a nanorod transmitted to vacuum. In the case of two infinite parallel cylinders, F_V is given by[27]

$$F_V = \varepsilon\left(\sqrt{h^2 - 4} - h + 2\arcsin(2/h)\right)\Big/2\pi, \quad (4)$$

where h is the ratio between the center-to-center nanorod spacing, s, and the radius, r. Because the length of each individual element, dz, is significantly longer than s and r, each adjacent pair of elements along the two nanorods was approximated as a pair of infinite parallel cylinders for the purposes of calculating F_V.

As with thermal conductivity, emissivity can vary significantly among different nanostructures. Thus, simulations were performed over a range of $\varepsilon = 0.05 - 0.21$ in order to investigate how stronger absorption would affect energy exchange between nanorods. The near-field effects amplifying radiative energy exchange relative to the amount calculated from the Stefan–Boltzmann equation were represented by a correction factor, F_{NF}. The magnitude of this factor with respect to the gap between the surfaces of the two nanorods was derived from a numerical study of radiative energy exchange between two Si nanorods, specifically the relative difference between the near-field energy exchange and the expected far-field contribution, as depicted in Fig. 3 of Ref. 11. This factor was fitted in a manner similar to that shown in Fig. 1(b) of Ref. 9. The 18–50 nm region was fitted to a C/g^{PF} relation, with g being the gap distance, C being a fitting constant, and PF being a power factor of 3.75. However, this fit would break down below 18 nm, a region unexplored by Ref. 9, where the gain in F_{NF} diminished with decreasing gap size [Fig. 3(b)]. That region was instead fitted to a double exponential relation to reflect this change. The region beyond 50 nm was fitted to a curve that would exponentially converge to an asymptote of 1 as in Ref. 9, representing transition to the far-field regime.

Trends in the peak temperature of the nanorod pair, with the same size and heating profile as those used for one nanorod above, are shown in Fig. 4. As the spacing between nanorods was reduced, the peak temperature rose nonlinearly. This effect was amplified with lower thermal conductivity [Fig. 4(a)] and higher emissivity [Fig. 4(b)], with emissivity having the stronger effect on temperature. The increase in temperature with higher emissivity correlated with an increase in the percentage of radiated energy from one nanorod absorbed by the other [Fig. 4(c)], indicating reduced heat dissipation to the surrounding vacuum environment.

Small nanorod array

For arrays consisting of more than two nanorods, the net radiative energy exchange for each nanorod was assumed to be the sum of individual contributions from all surrounding nanorods and the vacuum environment. This is expressed as

$$Q_{rad}(n) = F_{NF}\sigma\varepsilon(l/A)\left[T_1(n)^4 - \sum_2^L T_i(n)^4 F_{v,i} - T_0^4\left(1 - \sum_2^L F_{v,i}\right)\right]. \quad (5)$$

It is important to emphasize that the interactions between nanorods in the array are not limited to two-body effects; many-body interactions can substantially affect the outcome.[28–31] For example, such effects may further enhance radiative energy exchange compared to the situation in two-body systems, possibly due to the increased influence and concentration of surface plasmon polariton modes.[32]

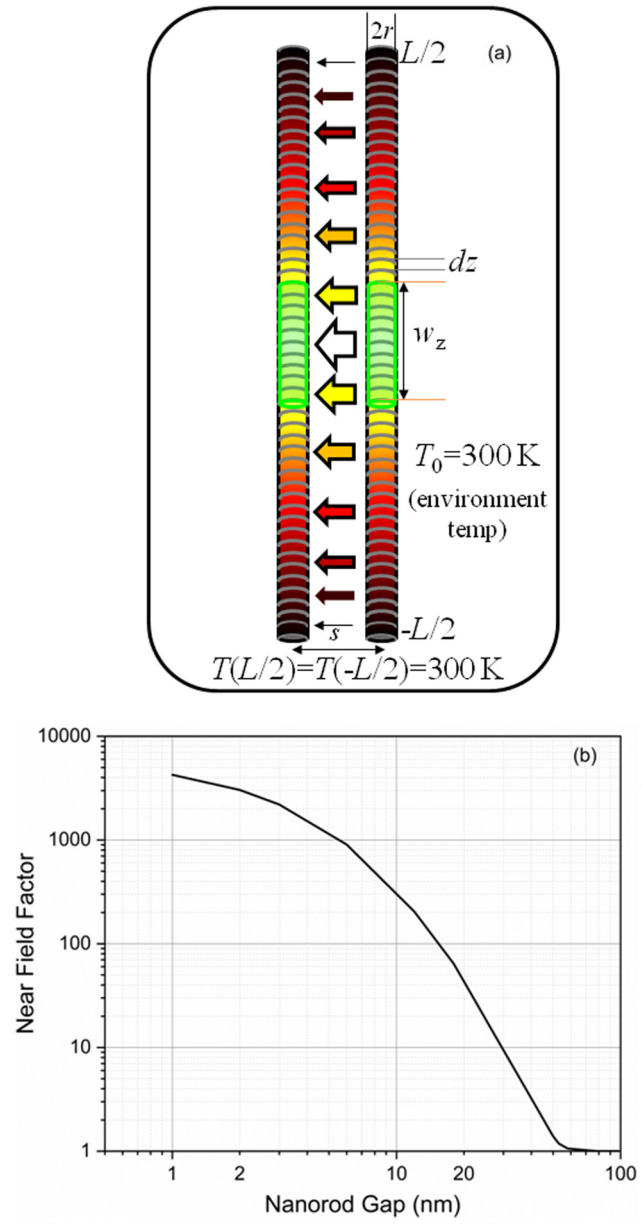

FIG. 3. (a) Schematic of heat flux (arrows) and finite difference discretization of two nanorods. (b) The near-field correction factor F_{NF} as a function of the gap between the surfaces of the two nanorods.

This is especially prevalent at very small gap distances (on the order of single nm), as shown in Ref. 31, where the projected enhancement between multi-body plates is far higher than suggested in Ref. 11 and Fig. 3(b). However, currently there are no reports on specific amplification values due to such effects with respect to gap distance for nanorods. Therefore, in the present study, we use only the two-body interaction above, while varying ε to observe how amplified radiative energy exchange may influence the temperature distribution.

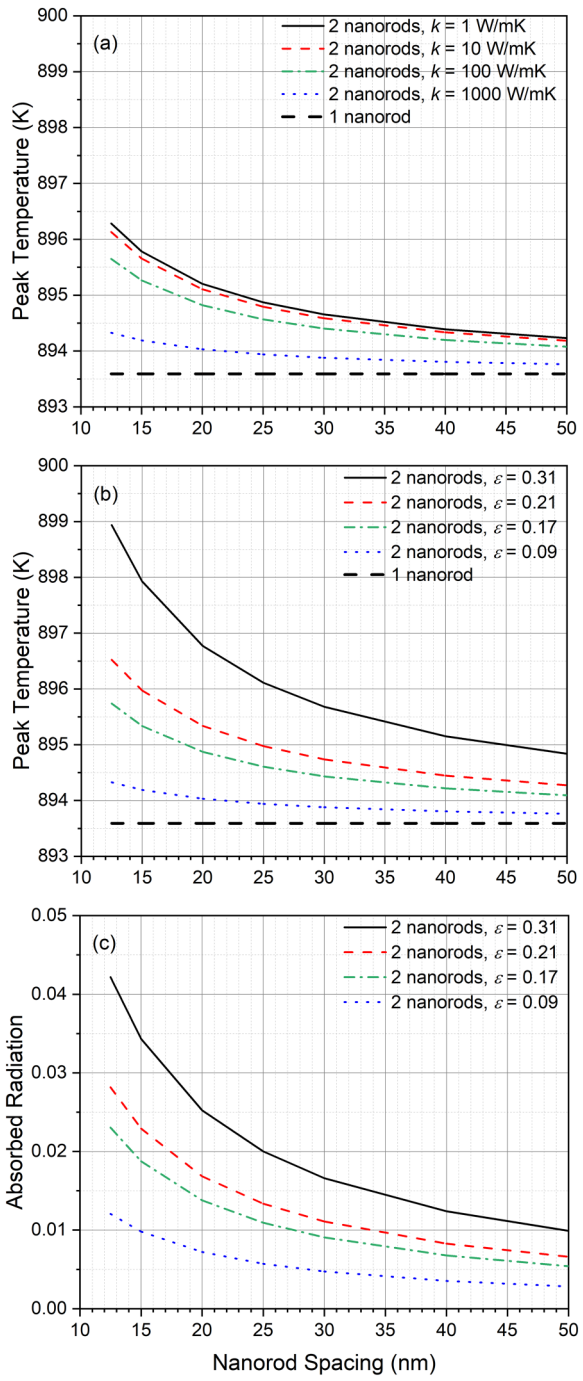

FIG. 4. Peak temperature as a function of center-to-center spacing between two nanorods, compared against the corresponding peak temperature for one isolated nanorod, for (a) varying thermal conductivity at a fixed emissivity value of 0.09 and (b) varying emissivity at a fixed thermal conductivity value of 1000 W/m K. In each case, the total heating power was chosen so as to yield the same peak temperature for one nanorod. The fraction of radiated emission absorbed by the other nanorod, F_V is plotted in (c) for varying emissivity.

To investigate radiative energy exchange within nanorod arrays, the two-nanorod system was expanded into a hexagonally close packed array with center-to-center CNT spacing fixed at 15 nm. With increasing array size, the peak temperature rose at a decreasing rate with respect to the total number of nanorods in the array (Fig. 5). Lower thermal conductivity and higher absorption would further amplify the rise in temperature, with both properties and array size having a multiplicative effect on the peak temperature. For the array with 37 nanorods, the temperature increased by

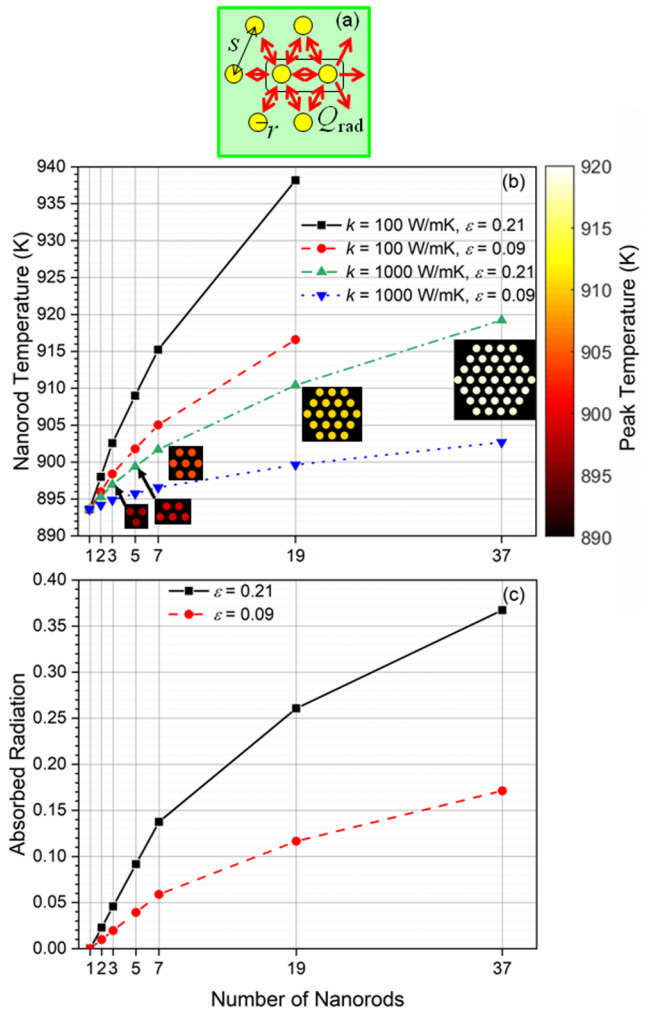

FIG. 5. (a) Top view schematic of a nanorod array, with the cross section of each nanorod represented by a circle. Red arrows indicate radiative energy exchange from the highlighted nanorods to the surrounding nanorods and vacuum as given in Eq. (5). (b) Peak temperature as a function of the number of nanorods in the array for various thermal conductivity and emissivity values. The inset images with filled circles show the top views of the arrays, with nanorods spaced 15 nm apart from each other and their color corresponding to the peak temperature on each nanorod. (c) Fraction of radiation emitted by the central nanorod absorbed by other nanorods.

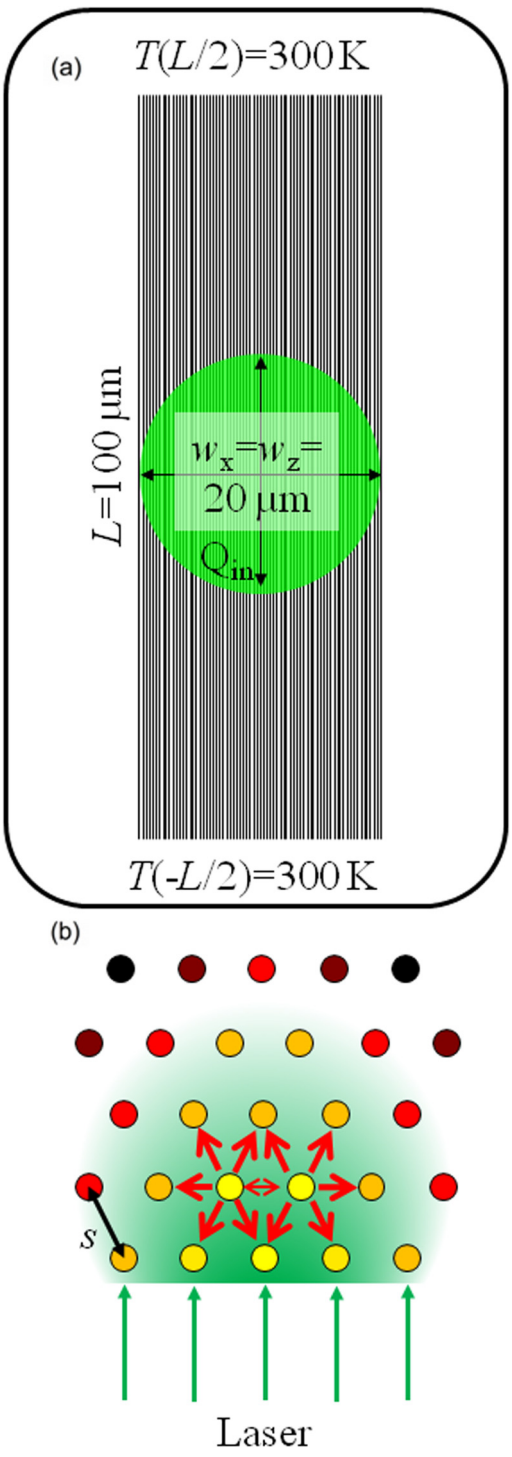

FIG. 6. Schematic of laser heating on a CNT forest side surface. Front view is shown in (a), and top view is shown in (b), with circles representing the cross sections of the CNTs. The colors are meant to give an impression of the temperature distribution within the CNT forest.

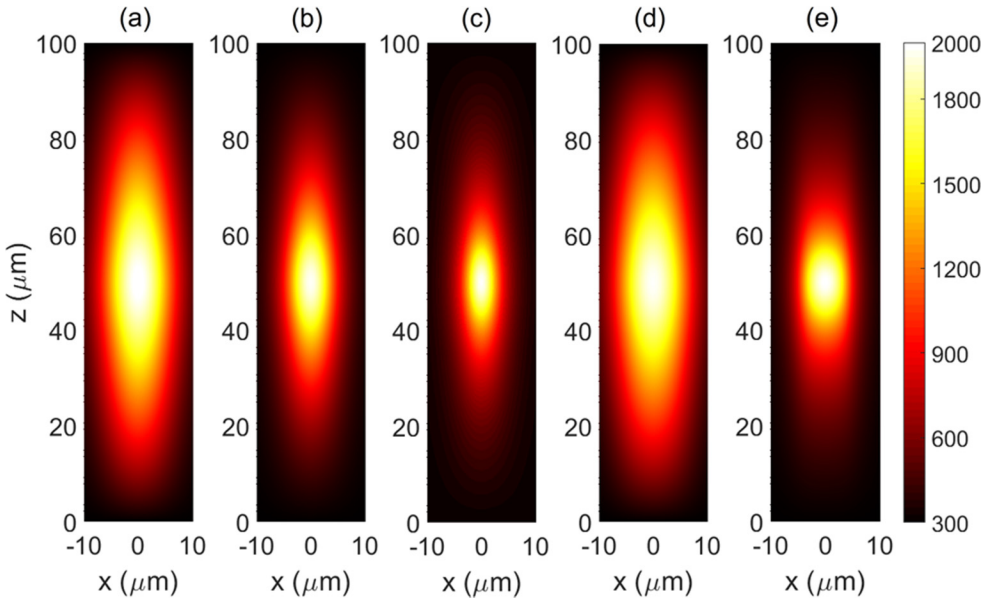

FIG. 7. Temperature distribution on the side surface of the CNT forest as a result of laser heating for the thermal conductivity models shown in Table I, with $\alpha = 3.7 \times 10^{-7}$ m/W and $\beta = 9.7 \times 10^{-10}$ m/W K. For (a)–(c), the thermal conductivity was 5000 W/m K at room temperature, while for (d)–(e), it was 100 W/m K at room temperature.

9 K for $k = 1000$ W/m K and 26 K for $k = 100$ W/m K. A comparable increase in temperature was observed when going from $\epsilon = 0.09$ to $\epsilon = 0.21$ [Fig. 5(b)], which was well correlated with the trend in the percentage of absorbed radiation within the array [Fig. 5(c)]. The combination of both $k = 100$ W/m K and $\epsilon = 0.21$ led to an even higher temperature rise where, in the case of the 19-nanorod array, the temperature increase was 44 K compared to a mere 6 K increase for $k = 1000$ W/m K and $\epsilon = 0.09$. The trend projects an even greater temperature rise with increasing array size and stronger radiative energy exchange (Fig. S3).

Optically heated CNT forest

The array was further expanded in order to simulate the experimental conditions for optical heating of the side surface of a CNT forest. Instead of a uniform spot for the external heating source, a Gaussian distribution with a $1/e^2$ beam diameter of 20 μm, emulating a focused laser beam, was implemented (Fig. 6). The 100-μm tall CNTs were arranged in a 5-row array with enough CNTs to completely cover the laser spot. The Q_{in} for the CNTs deeper in the array was attenuated by the CNTs the laser would pass through, with the attenuation determined by the CNT emissivity. Finally, we also explored the behavior of thermionic electron emission from the hot spot, which is of interest for electron sources and vacuum electronic applications. Based on the obtained temperature distribution, the thermionic electron emission current from the array, I, was estimated from the Richardson–Laue–Dushman equation integrated over the surface,

$$I = \oiint AT^2 \exp(-W/k_B T) dA, \tag{6}$$

where $A = 1.2 \times 10^6$ A/m^2 K^2, k_B is the Boltzmann constant, and W is the CNT work function (generally known to be around 4.5 eV). Because the electron path for most of the internal CNTs would be obstructed by other CNTs, I was calculated as a surface integral of the unobstructed front-half surfaces of the front row CNTs, where $dA = \pi r^2 dz$ is the emitting surface area of each discrete element. Such a selective integration is similar to the approach shown in Ref. 38.

To gain insight into how the temperature dependence of thermal conductivity affects the temperature distribution, three models were considered: a constant k of approximately 5000 W/m K, $k = (aT)^{-1}$, and $k = (\alpha T + \beta T^2)^{-1}$ (as first described in Fig. 2).[17] In each case, the thermal conductivity was approximately 5000 W/m K for $T = 300$ K. The center-to-center CNT spacing was set to 25 nm, the emissivity to 0.09, and a peak temperature of approximately 2000 K was targeted, a temperature that has been experimentally observed for multi-walled CNT field emitters.[39] As can be seen from the plots of Figs. 7(a)–7(c) and Table I, the spread of the temperature distribution area, as well as the total thermionic emission current dropped to approximately a quarter by going from constant k to $k = (aT)^{-1}$ and then $k = (\alpha T + \beta T^2)^{-1}$, but this was accompanied by a commensurate reduction in the laser power required to reach the same peak temperature.

Due to defects and inter-CNT interactions, the thermal conductivity of CNTs in large arrays is expected to be lower,[1,2,19] and their emissivity higher,[16] than those of pristine single CNTs. Thus, simulations were also carried out for thermal conductivity models with $k = 100$ W/m K at room temperature [Figs. 7(d) and 7(e)], which is close to the expected thermal conductivity for a defective CNT.[18] The temperature distribution shown in Fig. 7(d) for a constant k = 100 W/m K is similar to the $k = 5000$ W/m K case of Fig. 7(a), but with far less input power. Interestingly, the case shown in

TABLE I. Peak temperature, area of the CNT sidewall with temperature above the full-width at half maximum (FWHM) relative to 300 K, and total thermionic electron emission current for a CNT forest at varying thermal conductivity and laser power, with simulations labeled as shown in Fig. 7.

Simulation	a	b	c	d	e
Thermal conductivity (W/m K)	5000	1 500 000/T	$1/(\alpha T+\beta T^2)$	100	$1/[50(\alpha T+\beta T^2)]$
Laser power (mW)	518	174	106	11.4	2.7
Peak temperature (K)	1980	1980	1980	1990	2000
FWHM area (μm^2)	478	218	115	493	165
Emission current (pA)	469	203	88	521	209

Fig. 7(e) has a wider temperature spread in the horizontal direction than its higher conductivity counterpart of Fig. 7(c) and a corresponding increase in emission current (at a much-reduced input power). This widening of the temperature distribution seems to occur because, as longitudinal thermal conductivity becomes very low at high temperatures in the case of Fig. 7(e), each nanotube is heated to a higher temperature by the input laser beam. In addition, lateral heat exchange due to radiation becomes more prominent as the mechanism for the central nanotubes (which receive a higher input laser power compared to the rest of the array) to dissipate the energy they receive from the laser beam.

Further simulations were carried out using the thermal conductivity case in Fig. 7(c), with the inter-CNT spacing varied in order to investigate the impact of CNT density on the temperature distribution and, subsequently, thermionic emission current.[33] As Fig. 8 shows, for 5-nm-radius CNTs, the thermionic emission current peaked at a spacing of 25 nm, namely, five times the radius. This was due to a combination of two competing factors. For more closely spaced CNTs, strong near-field radiative energy exchange would lead to heat dissipation deeper into the array and, thus, lower peak temperature and thermionic emission current. For more loosely spaced CNTs, the peak temperature would not depend on CNT spacing, but the effective electron emission area would be reduced due to the lower number of CNTs contained within the laser spot.

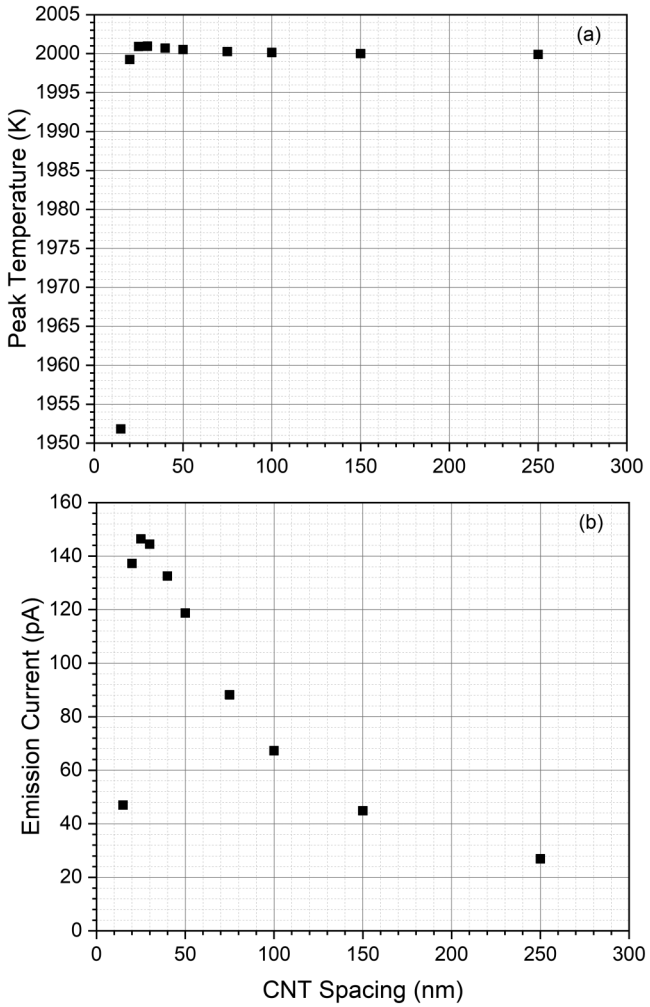

FIG. 8. (a) Peak temperature as a function of CNT spacing for a 5-row CNT array 20 μm in width and with $k=(\alpha T+\beta T^2)^{-1}$. (b) Thermionic emission current as a function of CNT spacing for the same array.[26]

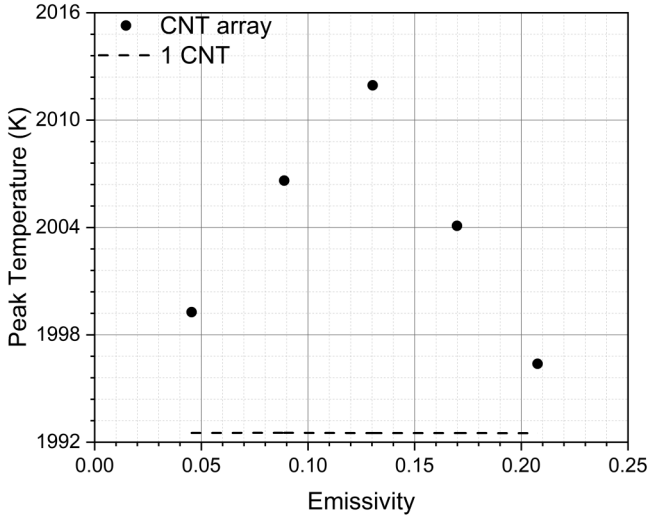

FIG. 9. Peak temperature increase for a 15 × 10 CNT array with $k = 100$ W/m K relative to a single CNT, as a function of emissivity. In each case, the total heating power was chosen so as to yield approximately the same peak temperature for one CNT.

The CNT emissivity was also varied within the range of $\varepsilon = 0.05 - 0.21$, and the peak temperature of the array was compared with the equivalent temperature for a single CNT (Fig. 9). The increase in peak temperature for the array was maximized at approximately $\varepsilon = 0.13$, where a balance would be achieved between laser energy penetration into the CNT array and inter-tube radiative energy exchange. As emissivity (and thus absorptivity) was increased, initially the peak temperature was increased, as expected; however, further increase in emissivity led to higher thermal radiation from the front-row nanotubes deep into the forest, thus increasing the overall heated volume and lowering the peak temperature of the array.

SUMMARY AND CONCLUSIONS

We presented a model for heat transport in nanorod arrays based on radiative energy exchange between pairs of nanorods and used it to investigate how those interactions may affect heat localization within the array across different scenarios. The temperature rise induced by radiative energy exchange among nanorods is greatly amplified by increased array size and reduced inter-nanorod distances, both of which reduce heat dissipation to the vacuum environment. Strong enhancements in heat localization in an array of nanorods were observed with lower thermal conductivity. For a single nanorod, extreme temperature localization could be observed at very low thermal conductivity, and similar localization enhancement could also be observed in a macro-scale nanorod assembly. The model also revealed unexpected results such as the peak temperature in a laser-heated array being a non-monotonic function of nanorod emissivity.

A previous simulation study[34] showed heat localization due to anisotropic thermal conduction in a bulk. The present study, using a microscopic model of arrays of 1D materials and explicit treatment of inter-rod radiative coupling, further confirms the possibility of heat localization being a property of 1D nanostructures. While such heat localization has been studied extensively in CNT forests,[15] it may well be a general property of 1D systems.[35] This could open up the possibility of using 1D nanomaterials other than CNTs with more suitable properties for various applications, such as lanthanum hexaboride nanowires with low work function[36] for thermionic emitters. Overall, these results show the model's potential in identifying qualitative relations between the structural and material properties of 1D nanostructures and their resultant temperature distribution. This can be further improved with more precise, in-depth simulation studies and experimental measurements regarding those relations, and will aid in identifying nanoengineering paths toward optimizing 1D nanostructures for various thermal applications, such as thermionic or thermoelectric energy conversion.[37]

SUPPLEMENTARY MATERIAL

See the supplementary material for expanded results related to Figs. 2 and 5, which further show the effects of emissivity on the temperature distribution.

DATA AVAILABILITY

The data that support the findings of this study are available within the article.

ACKNOWLEDGMENTS

We acknowledge financial support from the Natural Sciences and Engineering Research Council of Canada (NSERC) (Grant Nos. SPG-P-478867, RGPIN-2017-04608, and RGPAS-2017-507958). K.J.V acknowledges NSERC for a Postgraduate Doctoral Scholarship (Grant Nos. PGS-D-556043, PGS-D-576523, and PGS-D-597763). This research was undertaken thanks in part to funding from the Canada First Research Excellence Fund, Quantum Materials and Future Technologies Program.

REFERENCES

[1] A. M. Marconnet, M. A. Panzer, and K. E. Goodson, Rev. Mod. Phys. **85**, 1295 (2013).
[2] B. Kumanek and D. Janas, J. Mater. Sci. **54**, 7397 (2019).
[3] J. Xu and T. S. Fisher, Int. Soc. Conf. Therm. Phenom. **2**, 549 (2004).
[4] M. A. Peacock, C. K. Roy, M. C. Hamilton, R. W. Johnson, R. W. Knight, and D. K. Harris, Int. J. Heat Mass. Transf. **97**, 94 (2016).
[5] D. G. Cahill, P. V. Braun, G. Chen, D. R. Clarke, S. Fan, K. E. Goodson, P. Keblinski, W. P. King, G. D. Mahan, A. Majumdar, H. J. Maris, S. R. Phillpot, E. Pop, and L. Shi, Appl. Phys. Rev. **1**, 011305 (2014).
[6] M. Francoeur, M. P. Mengüç, and J. Quant, Spectrosc. Radiat. Transfer **109**, 280 (2008).
[7] K. Joulain, J. P. Mulet, F. Marquier, R. Carminati, and J. J. Greffet, Surf. Sci. Rep. **57**, 59 (2005).
[8] D. Thompson, L. Zhu, R. Mittapally, S. Sadat, Z. Xing, P. McArdle, M. M. Qazilbash, P. Reddy, and E. Meyhofer, Nature **561**, 216 (2018).
[9] R. St-Gelais, L. Zhu, S. Fan, and M. Lipson, Nat. Nano **11**, 515 (2016).
[10] R. Kubo, Rep. Prog. Phys. **29**, 255 (1966).
[11] L. Carrillo, Y. Bayazitoglu, and J. Quant, Spectrosc. Radiat. Transfer **112**, 412 (2011).
[12] P. Vincent, S. T. Purcell, C. Journet, and V. T. Binh, Phys. Rev. B **66**, 075406 (2002).
[13] P. Yaghoobi, M. V. Moghaddam, and A. Nojeh, Solid State Commun. **151**, 1105 (2011).
[14] A. H. Khoshaman, H. D. E. Fan, A. T. Koch, G. A. Sawatzky, and A. Nojeh, IEEE Nano. Magn. **8**, 4 (2014).
[15] A. Nojeh, MRS Bull. **42**, 500 (2017).
[16] H. Ye, X. J. Wang, W. Lin, C. P. Wong, and Z. M. Zhang, Appl. Phys. Lett. **101**, 141909 (2012).
[17] E. Pop, D. Mann, Q. Wang, K. Goodson, and H. Dai, Nano Lett. **6**, 96 (2006).
[18] C. Sevik, H. Sevinçli, G. Cuniberti, and T. Çağın, Nano Lett. **11**, 4971 (2011).
[19] A. E. Aliev, M. H. Lima, E. M. Silverman, and R. H. Baughman, Nanotechnology **21**, 035709 (2010).
[20] P. Martin, Z. Aksamija, E. Pop, and U. Ravaioli, Phys. Rev. Lett. **102**, 125503 (2009).
[21] R. S. Prasher, X. J. Hu, Y. Chalopin, N. Mingo, K. Lofgreen, S. Volz, F. Cleri, and P. Keblinski, Phys. Rev. Lett. **102**, 105901 (2009).
[22] S. Berber, Y. K. Kwon, and D. Tomanek, Phys. Rev. Lett. **84**, 4613 (2000).
[23] V. A. Golyk, M. Krüger, and M. Kardar, Phys. Rev. E **85**, 046603 (2012).
[24] Y. Fan, S. B. Singer, R. Bergstrom, and B. C. Regan, Phys. Rev. Lett. **102**, 187402 (2009).
[25] J. Liu, T. Li, Y. Hua, and X. Zhang, Nanoscale **9**, 1496 (2017).
[26] R. R. Nair, P. Blake, A. N. Grigorenko, K. S. Novoselov, T. J. Booth, T. Stauber, N. M. R. Peres, and A. K. Geim, Science **320**, 1308 (2008).
[27] J. R. Howell, *A Catalog of Radiation Configuration Factors* (McGraw-Hill, 1982).
[28] M. Kruger, G. Bimonte, T. Emig, and M. Kardar, Phys. Rev. B **86**, 115423 (2012).

[29]I. Latella, P. Ben-Abdallah, S.-A. Biehs, M. Antezza, and R. Messina, Phys. Rev. B **95**, 205404 (2017).
[30]M. Nikbakht, Phys. Rev. B **96**, 125436 (2017).
[31]I. Latella, S. Biehs, R. Messina, A. W. Rodriguez, and O. Ben-Abdallah, Phys. Rev. B **97**, 035423 (2018).
[32]Y. H. Kan, C. Y. Zhao, and Z. M. Zhang, Phys. Rev. B **99**, 035433 (2019).
[33]K. J. Voon, M. Chang, G. A. Sawatzky, and A. Nojeh, in *Proceedings of 32nd International Vacuum and Nanoelectronics Conference* (IVNC, Cincinnati, 2019).
[34]M. Chang, H. D. E. Fan, M. M. Chowdhury, G. A. Sawatzky, and A. Nojeh, Phys. Rev. B **98**, 155422 (2018).
[35]M. Chang, M. Dahmardeh, M. V. Moghaddam, S. M. Mirvakili, J. D. W. Madden, K. Takahata, A. Nojeh, in *Proceedings of 58th International Conference on Electron Ion Photon Beam Technology and Nanofabrication*, (EIPBN, 2014), P02-02.
[36]J. Xu, Y. Zhao, and C. Zou, Chem. Phys. Lett. **423**, 138 (2006).
[37]A. H. Khoshaman, H. D. E. Fan, A. T. Koch, and G. A. Sawatzky, IEEE Nanotechnol. Magn. **8**(2), 4 (2014).
[38]G. Tripathi, J. Ludwick, M. Cahay, and K. L. Jensen, private communication (2020).
[39]S. T. Purcell, P. Vincent, C. Journet, and V. T. Binh, Phys. Rev. Lett. **88**(10), 105502 (2002).